Ultrahigh sensitive sub-terahertz detection by InP-based asymmetric dual-grating-gate high-electron-mobility transistors and their broadband characteristics

Y. Kurita, Guillaume Ducournau, D. Coquillat, A. Satou, K. Kobayashi, S. Boubanga-Tombet, Y.M. Meziani, V.V. Popov, W. Knap, T. Suemitsu, et al.

Applied Physics Letters

Ultrahigh sensitive sub-terahertz detection by InP-based asymmetric dual-grating-gate high-electron-mobility transistors and their broadband characteristics

Cite as: Appl. Phys. Lett. **104**, 251114 (2014); https://doi.org/10.1063/1.4885499
Submitted: 31 March 2014 • Accepted: 15 June 2014 • Published Online: 25 June 2014

Y. Kurita, G. Ducournau, D. Coquillat, et al.

Ultrahigh sensitive sub-terahertz detection by InP-based asymmetric dual-grating-gate high-electron-mobility transistors and their broadband characteristics

Y. Kurita,[1] G. Ducournau,[2] D. Coquillat,[3] A. Satou,[1,a)] K. Kobayashi,[1] S. Boubanga Tombet,[1] Y. M. Meziani,[4] V. V. Popov,[5] W. Knap,[3] T. Suemitsu,[1] and T. Otsuji[1]
[1]*Research Institute of Electrical Communication, Tohoku University, 2-1-1 Katahira, Aoba-ku, Sendai 980-8577, Japan*
[2]*Institut d'Electronique, de Microélectronique et de Nanotechnologie, 59562 Villeneuve d'Ascq Cedex, France*
[3]*Laboratoire Charles Coulomb, UMR 5221, Université Montpellier 2 - CNRS, F-34095 Montpellier, France*
[4]*Departamento de Fisica Aplicada, Universidad de Salamanca, Salamanca 37008, Spain*
[5]*Kotelnikov Institute of Radio Engineering and Electronics, 410019 Saratov, Russia*

(Received 31 March 2014; accepted 15 June 2014; published online 25 June 2014)

We report on room-temperature plasmonic detection of sub-terahertz radiation by InAlAs/InGaAs/InP high electron mobility transistors with an asymmetric dual-grating-gate structure. Maximum responsivities of 22.7 kV/W at 200 GHz and 21.5 kV/W at 292 GHz were achieved under unbiased drain-to-source condition. The minimum noise equivalent power was estimated to be 0.48 pW/Hz$^{0.5}$ at 200 GHz at room temperature, which is the record-breaking value ever reported for plasmonic THz detectors. Frequency dependence of the responsivity in the frequency range of 0.2–2 THz is in good agreement with the theory. © *2014 AIP Publishing LLC*.
[http://dx.doi.org/10.1063/1.4885499]

Plasmonic terahertz (THz) detectors taking advantage of hydrodynamic nonlinearities in two-dimensional (2D) electron channels of the field effect transistors (FETs) were initially proposed in Ref. 1. The plasmonic detectors have potentially higher sensitivity than the electron-transit detectors like Schottky barrier diodes (SBDs)[2] and faster response than that of the thermal detectors like Golay cells,[3] bolometers,[4] and pyroelectric detectors.[5]

Recently, development of the plasmonic detectors has been remarkably progressing. Responsivity of Si-FET integrated with an on-chip bow-tie antenna has reached 5 kV/W at 292 GHz.[6] Gallium nitride high electron mobility transistor (HEMT) with a narrowband dipole antenna incorporated with the gate and source electrodes has demonstrated responsivity of 1.1 kV/W at 1 THz.[7] Furthermore, very high responsivity of 2.2 kV/W at 1 THz was demonstrated using InAlAs/InGaAs/InP HEMT with an asymmetric dual-grating-gate (A-DGG).[8,9] Such enormous responsivity of the A-DGG HEMT THz detector was achieved due to its intense nonlinear rectification response and strong coupling between incident THz radiation and plasmons in 2D electron channels of the A-DGG HEMT. However, the detection using the A-DGG HEMT in the sub-THz region has not been studied so far.

In this paper, we report on ultrahigh values of responsivity exceeding 20 kV/W and excellent noise equivalent power (NEP) below 1 pW/Hz$^{0.5}$ for sub-THz detection (200 GHz and 292 GHz) at room temperature by the A-DGG HEMT. We also study the frequency dependence of the responsivity in the frequency range of 0.2–2 THz. The experimentally obtained results agree qualitatively with the theoretical predictions.[10]

Terahertz plasmonic photoresponse in the FET channels originates from the nonlinear dynamics of 2D electron fluid described by the hydrodynamic equations.[1] In the A-DGG HEMT, the rectified DC photocurrent originates from two different plasmonic effects: the plasmonic drag and plasmonic ratchet (2D plasmonic electrostriction) effects.[8,10] The rectified DC photocurrent density, Δj, gives rise to an output photovoltage ΔU between the drain and source contacts, $\Delta U = -WR_{ds}\Delta j$, where W is the width of the FET, and R_{ds} is the channel DC resistance between the drain and source contacts.

The photovoltage ΔU can be greatly enhanced in A-DGG HEMT structure (see Fig. 1(a)). By setting one of

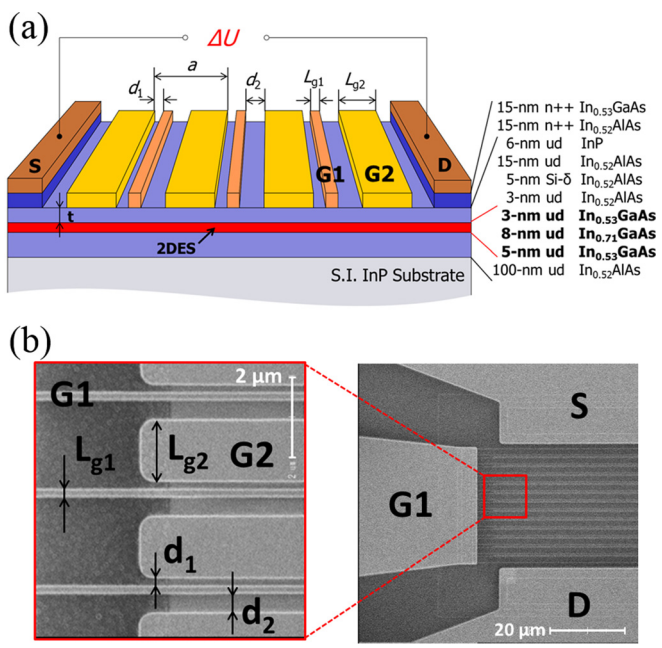

FIG. 1. (a) A schematic view of the A-DGG HEMT. (b) SEM images of the A-DGG HEMT.

a)E-mail: a-satou@riec.tohoku.ac.jp

the gate voltages to create plasmonic cavities underneath the corresponding gates and another one to almost deplete the other regions of the channel, one can obtain both high photocurrent induced in the cavities and high channel resistance in the strongly depleted regions simultaneously. In this case, the DGG structure forms a cascade connection of the multiple depleted regions, thus realizing a high net output photovoltage as the sum of the photovoltages generated in each unit cell. The A-DGG also works as an efficient broadband coupler in THz region between the incident electromagnetic wave and the plasmons in the 2D electron channel.[11]

Asymmetric unit cell of the A-DGG HEMT structure plays a key role for allowing zero drain bias detection, because it makes unbalance of the impedances between adjacent gate fingers, so that the photocurrent generated in 2D plasmonic cavities by incident THz radiation performs unilateral transport from the source to drain, resulting in summing up the photovoltaic signals. In a symmetric DGG structure, identical impedances between the adjacent gate fingers cancel out the generated photovoltaic signals. Small responsivities (<100 V/W) for zero drain bias reported for symmetric-DGG HEMTs[12,13] could possibly originate from a slight asymmetry in the DGG structure that was unintentionally caused by fabrication process-dependent variations.

A-DGG HEMTs were designed and fabricated using InAlAs/InGaAs/InP material systems. Figures 1(a) and 1(b) show the schematic view and typical scanning electron microscope (SEM) images of A-DGG HEMTs, respectively. Two types of A-DGGs, consisting of gate fingers G_1 (with length L_{g1}) and gate fingers G_2 (with length L_{g2}), were formed with 156-nm thick Ti/Au. The 2D electron channel is formed in a 16-nm-thick, undoped InGaAs layer sandwiched between undoped InAlAs barrier layers; the upper barrier layer contains remote-doping layer inside. The electron density in the channel is $2.5 \times 10^{12}\,\mathrm{cm}^{-2}$ with the electron effective mass $m = 0.043m_0$ (m_0 is the free-electron mass) and the electron mobility $\mu = 11\,000\ \mathrm{cm}^2/\mathrm{V\ s}$ at room temperature, respectively. The geometrical parameters of the A-DGG HEMTs studied in this work are summarized in Table I. The asymmetry factor, the ratio of the interfinger spaces, d_1/d_2 was set to be 0.5. The chirped grating gates G_1 (215–430 nm) are introduced in sample #2 to unify the plasmon resonant frequencies over the entire plasmon cavities under gates G_1[14] at a certain drain bias, while all gates G_1 of the sample #1 have an identical length (200 nm). However, in this work, the non-resonant detection with zero drain-to-source bias is studied (see below), so that the effect of the chirped structure on the responsivity could be neglected.

We evaluated the detection performance of the A-DGG HEMTs to electromagnetic radiations at 200 and 292 GHz at room temperature. The schematic of 200-GHz detection system is described in Ref. 15. The continuous-wave (CW) THz source has the output power of 2.8 mW and a spot size of 2 mm in diameter. The THz radiation was focused onto the surface of the device by two polymethylpentene (TPX) lenses. The 292-GHz detection measurement was conducted using the experimental system similar to that described in Ref. 6. Terahertz beam with power 2 mW was focused on the surface of the device (with the beam spot diameter of 4 mm) by parabolic mirrors. Both sub-THz sources were produced using a microwave signal-generator and multipliers. The photovoltage ΔU generated by THz rectification at the drain with respect to the source was observed by a lock-in amplifier technique.

TABLE I. Geometrical parameters of the A-DGG HEMT samples.

Sample #	1	2
L_{g1} (nm)	200	215–430
d_1/d_2 (nm)	200/400	200/400
L_{g2} (nm)	1600	1600
No. of fingers: G_1/G_2	8/9	8/9
Active area (μm^2)	20×20	20×20

The responsivity, R_v, of the plasmonic detector is defined as

$$R_v = \frac{S_t \Delta U}{S_d P_t}, \tag{1}$$

where ΔU is the measured photovoltage, P_t is the total power of the THz radiation in the detector plane, S_t is the spot size of the radiation beam, and S_d is the active area of the plasmonic detectors. Note that the normalization factor S_t/S_d, which is much larger than unity for the A-DGG HEMTs fabricated in this work, appears here in contrast to the measured responsivity, $\Delta U/P_t$. This is to demonstrate the intrinsic performance of the plasmonic detectors that could be obtained if the entire power of incident THz radiation would be focused on the active area by the implementation of a perfectly matched antenna and/or a sufficiently large active area.

The plasmonic detectors have two types of detection modes depending on the value of the quality factor, $Q = \omega\tau$, where ω is the angular frequency of the incident wave, and τ is the electron momentum relaxation time. A resonant (frequency-tunable) mode takes place when $\omega\tau \gg 1$. On the other hand, when $\omega\tau \ll 1$ it gives rise to a non-resonant mode. With $\tau = m\mu/e = 0.27$ ps for our detectors, where e is the electron charge, the non-resonant-type behavior is expected for room-temperature sub-THz detection. This value of τ gives a quality factor of $\omega\tau = 0.34/0.50$ at 200/292 GHz, respectively. Figure 2(a) shows the responsivities of A-DGG HEMTs observed at room temperature as a function of the gate voltage V_{g2} (V_{g1} is zero). Measurements were conducted under zero drain-to-source bias condition to minimize the noise. The maximum responsivity for the sample #1 excited at 200 GHz was around 22.7 kV/W for $V_{g2} = -0.9$ V which is close to the threshold voltage and 21.5 kV/W for sample #2 excited at 292 GHz. These are the record-breaking values ever reported for plasmonic THz detectors in this frequency region.

On the other hand, relatively lower responsivities of 2.1 kV/W and 0.4 kV/W for 200 GHz and 292 GHz, respectively, were obtained when V_{g1} was varied and V_{g2} was fixed at zero value (Fig. 2(b)). In this case, the regions under gates G_1 (having the gate length L_{g1}) are depleted. The length L_{g1} of samples #1 and #2 are 200 nm and from 215 to 430 nm, respectively, which are much shorter than the length L_{g2} (1600 nm). This reduces the channel resistance R_{ds}, resulting in weaker responsivity. Note that the length of the plasmonic

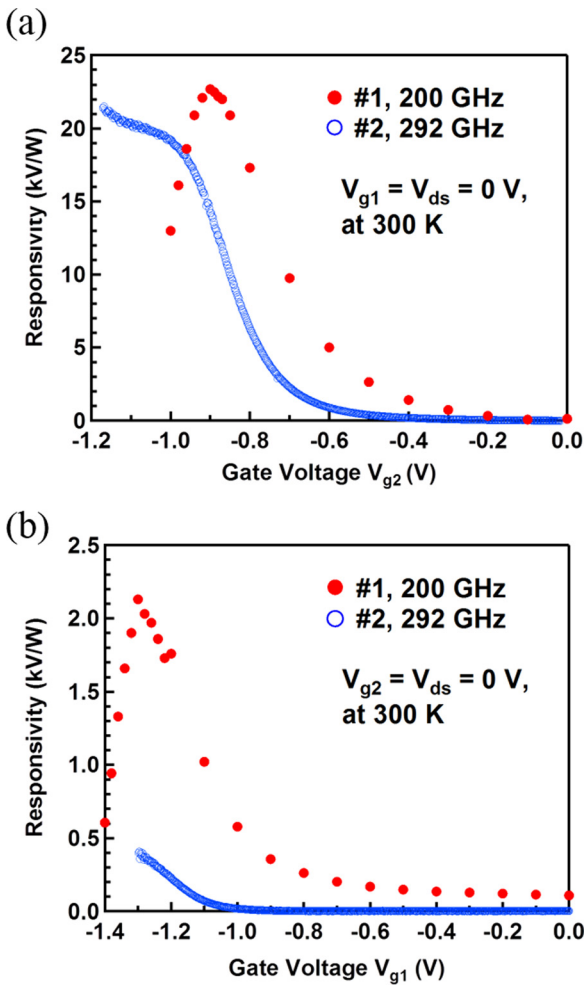

FIG. 2. Responsivity measured at 200 GHz and 292 GHz at room temperature for samples #1 and #2 as a function of (a) V_{g2} (for $V_{g1} = 0$) and (b) V_{g1} (for $V_{g2} = 0$).

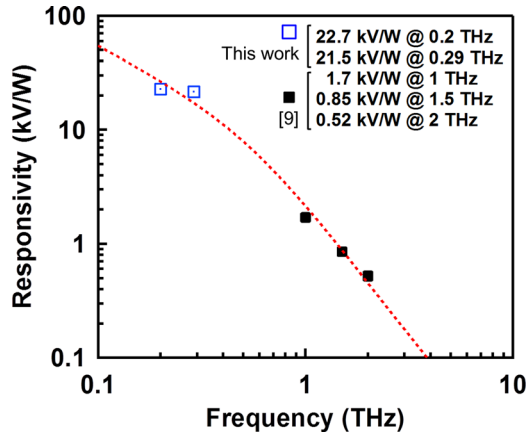

FIG. 3. Log-Log plot of responsivity as a function of frequency. Measurements in Ref. 9 were performed on a sample with geometrical parameters identical to sample #2. The responsivity at 200 and 292 GHz were measured on samples #1 and #2, respectively (sample #1 differs from #2 only by the chirped gate fingers G_1, the effect of which on the responsivity can be neglected; see the corresponding discussion in the text). The red curve is the fitting based on the formulas of Ref. 10 for the overall responsivity resulted from the plasmonic drag and plasmonic ratchet effects taking into account the Drude absorption frequency-dependent factor.

cavities created under the unbiased gates, which determines the resonant plasmon frequency of the resonant detection mode, is expected to have less influence on the photocurrent in the broadband detection mode studied here.

Figure 3 shows the log-log plot of the responsivities measured in this work (at 200 and 292 GHz) and the previous work (at 1–2 THz)[9] as a function of the incident THz radiation frequency. Measurements in Ref. 9 were performed on the sample with geometrical parameters identical to sample #2. The responsivities at 200 and 292 GHz were measured on samples #1 and #2, respectively (sample #1 differs from #2 only by the chirped gate fingers G_1, the effect of which on the responsivity can be neglected; see the corresponding discussion above). The responsivity weakly depends on the frequency at lower frequencies (0.1–0.3 THz), while it decreases approximately as the inverse square of the frequency, ω^{-2}, in higher frequency region. The frequency dependent factors of the responsivity were studied in Ref. 10 for the plasmonic drag as well as for plasmonic ratchet rectification mechanisms, both acting in the A-DGG HEMT structure. According to Ref. 10, the plasmonic drag photocurrent normalized to the THz power absorbed per unit area of 2D electron channel is proportional to ω^{-1}, whereas that of the plasmonic ratchet is frequency independent. The absorbed power is proportional to a real part of the channel conductivity $\mathrm{Re}[\sigma(\omega)]$, where $\sigma(\omega) = e^2 N_0 \tau/[m(1 - i\omega\tau)]$ with N_0 being the average electron density in 2D electron channel. This gives an additional frequency dependent factor $1/(1 + \omega^2\tau^2)$ for both the plasmonic drag and plasmonic ratchet responsivities, corresponding to an inverse-square-frequency dependence in the high frequency region $\omega\tau \gg 1$. The value $\tau = 0.27$ ps (which is characteristic value for the InGaAs electron channel at 300 K) gives the cutoff frequency $f_c = 1/(2\pi\tau) \approx 590$ GHz clearly seen in Fig. 3. Thus, the frequency dependence of the experimentally obtained responsivities demonstrates good agreement with the fitting curve corresponding to the theoretical predictions of Ref. 10 for the overall responsivity resulted from both plasmonic drag and plasmonic ratchet effects. The observed values of the responsivity exceeding 20 kV/W at sub-THz frequency range are also quite reasonable as being achieved due to great enhancement of the plasmonic drag rectified photocurrent at lower (sub-THz) frequencies[10] and strong coupling between the incident THz wave and plasmons in the 2D electron channel ensured by the A-DGG.[11] It is worth mentioning that the responsivity value resulted from the plasmonic drag and plasmonic ratchet effects reported in this paper is by several orders of magnitude greater than that observed for the photonic drag[16] and thermoelectric ratchet effects in semiconductor heterostructures with 2D electron channels[17] and predicted for graphene.[18]

NEP is also an important figure of merit for evaluating the detection performance. It can be calculated as a ratio of noise factors over the responsivity, $\mathrm{NEP} = N/R_v$, where N is the sum of all possible noise factors. Analysis of I-V characteristics of our samples showed that we have contributions from both the thermal noise, $N_{th} = \sqrt{4k_B T_e R_c}$, and the shot noise caused by the gate leakage current, $N_{sh} \approx \sqrt{2eI_g R_c}$, where R_c is the channel resistance, T_e is the electron temperature, and I_g is the gate leakage current with zero drain-to-source bias (while either gates G_1 or gates G_2 are biased). Here, we assume that the electron temperature is equal to the

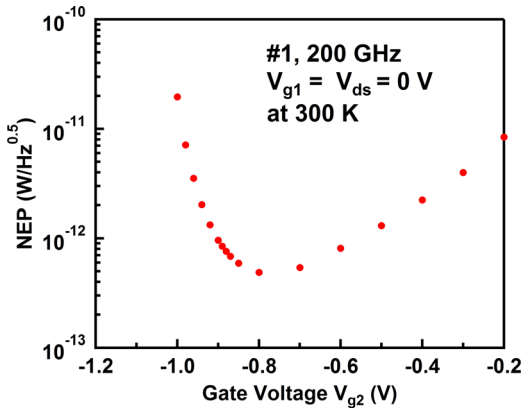

FIG. 4. NEP calculated for sample #1 at 200 GHz at room temperature.

room temperature. The expression for the latter noise was derived by assuming that the leakage current fully contributes to the noise as if the same value of the drain-to-source current flows through the channel. The channel resistance R_c at each gate voltage can be roughly estimated as follows. First, we model the A-DGG HEMT as a circuit that has two resistances, $R_s = R_c/2$ and $R_d = R_c/2$, connecting the source and drain terminals and the "gate resistance," R_g, connecting their middle to the gate terminal. Then, we calculate R_c from measured values of drain and gate currents at several bias points of V_{ds} and extrapolate it to $V_{ds} = 0$. Figure 4 shows the NEP estimated for sample #1 at 200 GHz with $V_{g1} = 0$. With setting the applied gate voltage V_{g2} closer to the threshold voltage, the responsivity rises very rapidly and the NEP decreases accordingly. Driving the A-DGG HEMT further to the sub-threshold region ($V_{g2} < -0.8$ V) leads to enhancing the NEP due to drastic rise in the channel resistivity. As a result, the obtained minimum value of the NEP is 0.48 pW/Hz$^{0.5}$. Such a low NEP is achieved in the A-DGG HEMTs owing to its high responsivity, while keeping the noise on the same level as in unbiased SBDs, down to around 10 nV/Hz$^{0.5}$ (cf. Ref. 19). This fact, together with high responsivity of our detector, demonstrates the excellent performance of the A-DGG HEMT THz detector far beyond existing plasmonic detectors in the sub-THz frequency region.

Room temperature sub-THz detection by InAlAs/InGaAs/InP A-DGG HEMTs was experimentally demonstrated. The obtained maximum responsivities exceeded 20 kV/W for both 200 GHz and 292 GHz. In addition, the minimum NEP of 0.48 pW/Hz$^{0.5}$ was estimated at 200 GHz. These are record-breaking values ever reported for plasmonic THz detectors. Nonlinear rectification response and excellent coupling efficiency provided by the A-DGG structure contributed to the drastic improvement on detection performances.

The authors thank T. Kawasaki from Research Institute of Electrical Communication, Tohoku University, for his helpful comments about the NEP estimation. The authors thank NTT-AT Corp. for cooperation in processing the sample fabrications. This work has been supported in part by the JST/ANR "WITH," a Japan-France strategic collaborative research project. The experiment was conducted in IEMN, Univ. Lille 1, Lille, France and LC2-Labs., Univ. Montpellier 2, Montpellier, France. Y.M.M. acknowledges the financial support from the MINECO through the Project No. TEC2012-32777. V.V.P. acknowledges the support the Russian Foundation for Basic Research through Grant Nos. 12-02-00813 and 14-02-92102.

[1]M. Dyakonov and M. Shur, IEEE Trans. Electron Devices **43**, 380 (1996).
[2]E. R. Brown, A. C. Young, J. E. Bjarnason, J. D. Zimmerman, A. C. Gossard, and H. Kazemi, Int. J. High Speed Electron. Syst. **17**, 383 (2007).
[3]M. J. E. Golay, Rev. Sci. Instrum. **18**, 347 (1947).
[4]P. L. Richard, J. Appl. Phys. **76**, 1 (1994).
[5]R. W. Whatmore, Rep. Prog. Phys. **49**, 1335 (1986).
[6]F. Schuster, D. Coquillat, H. Videlier, M. Sakowicz, F. Teppe, L. Dussopt, B. Giffard, T. Skotnicki, and W. Knap, Opt. Express **19**, 7827 (2011).
[7]T. Tanigawa, T. Onishi, S. Takigawa, and T. Otsuji, *Proceedings of the 68th Device Research Conference Digest, Notre Dame, IN, 21–23 June, 2010*, p. 167.
[8]V. V. Popov, D. V. Fateev, T. Otsuji, Y. M. Meziani, D. Coquillat, and W. Knap, Appl. Phys. Lett. **99**, 243504 (2011).
[9]T. Watanabe, S. Boubanga-Tombet, Y. Tanimoto, Y. Wang, H. Minamide, H. Ito, D. Fateev, V. V. Popov, D. Coquillat, W. Knap, Y. M. Meziani, and T. Otsuji, Solid State Electron. **78**, 109 (2012).
[10]V. V. Popov, Appl. Phys. Lett. **102**, 253504 (2013).
[11]T. Otsuji, M. Hanabe, T. Nishimura, and E. Sano, Opt. Express **14**, 4815 (2006).
[12]D. Coquillat, S. Nadar, F. Teppe, N. Dyakonova, S. Boubanga-Tombet, W. Knap, T. Nishimura, Y. M. Meziani, T. Otsuji, V. V. Popov, and G. M. Tsymbalov, Opt. Express **18**, 6024 (2010).
[13]A. El Moutaouakil, T. Suemitsu, T. Otsuji, H. Videlier, S. Boubanga-Tombet, D. Coquillat, and W. Knap, Phys. Status Solidi C **8**, 346 (2011).
[14]T. Nishimura, N. Magome, H.-C. Kang, and T. Otsuji, IEICE Trans. Electron. **E92-C**, 696 (2009).
[15]A. Westlund, P. Sangaré, G. Ducournau, P.-Å. Nilsson, C. Gaquiére, L. Desplanque, X. Wallart, and J. Grahn, Appl. Phys. Lett. **103**, 133504 (2013).
[16]W. Weber, L. E. Golub, S. N. Danilov, J. Karch, C. Reitmaier, B. Wittmann, V. V. Bel'kov, E. L. Ivchenko, Z. D. Kvon, N. Q. Vinh, A. F. G. van der Meer, B. Murdin, and S. D. Ganichev, Phys. Rev. B **77**, 245304 (2008).
[17]P. Olbrich, E. L. Ivchenko, R. Ravash, T. Feil, S. D. Danilov, J. Allerdings, D. Weiss, D. Schuh, W. Wegscheider, and S. D. Ganichev, Phys. Rev. Lett. **103**, 090603 (2009).
[18]A. V. Nalitov, L. E. Golub, and E. L. Ivchenko, Phys. Rev. B **86**, 115301 (2012).
[19]R. Han, Y. Zhang, D. Coquillat, H. Videlier, W. Knap, E. Brown, and K. K. O, IEEE J. Solid-State Circuits **46**, 2602 (2011).